Design of Antipodal Vivaldi Antenna for Medical Imaging Application

Daffa Mahendra [a], Randy Ivanal Hakim [b], and Endarko [c, *]

Laboratory of Medical Physics and Biophysics, Department of Physics,
Institut Teknologi Sepuluh Nopember
Kampus ITS Sukolilo, Klampis Ngasem, Sukolilo Surabaya 60111, Indonesia

e-mail: [a] dffmahendra12@gmail.com, [b] randyhakim8@gmail.com, and [c] endarko@physics.its.ac.id
* Corresponding Author

Abstract

The microwave imaging (MWI) system in medical applications is commonly used to detect abnormalities in the human body. The purpose of this study was to design an Antipodal Vivaldi Antenna (AVA) for medical imaging applications using MWI. The research method used is based on the AVA design simulation of the CST Studio Suite 2019 application using time and frequency domain methods, which has dimensions of 60x40 mm² with an antenna structure that works in the frequency range of 6.3-9.6 GHz, the impedance for bandwidth is -10 dB, using Flame Retardant-4 (FR-4) thickness 1.6 mm (ε_r = 4.3, tan δ = 0.025) as substrate material. A linear array of antennas was utilized in the simulation, either with or without a phantom. The phantom options include an absence of a phantom (only antennas), a cube-shaped water phantom, and a water phantom containing an anomaly. The result of the simulation on the AVA design produces a bandwidth of 41.61%, a gain of 5.16 dB, a return loss of -26.73 dB, a Specific Absorption Rate (SAR) value of 0.26 W/kg and a graph of S-parameters (S21). It can be concluded that the MWI system using the AVA design in this study has the potential to properly detect the presence of anomalies.
Keywords: *Microwave Imaging; Specific Absorption Rate; Vivaldi Antenna*

INTRODUCTION

Medical imaging systems have been widely used in conventional radiology devices such as X-rays, CT scans, and MRIs to diagnose abnormalities in the human body [1]. These devices utilize ionizing radiation as the irradiation method to distinguish normal and abnormal tissue parameters. However, excessive exposure to ionizing radiation can cause damage to normal tissue, leading to ionizing effects [2]. To address this issue, the MWI technique, a safer, non-ionizing, non-invasive, and relatively cost-effective alternative, has been introduced [3].

MWI produces images of human body tissues using microwave signals. The operation involves a tool that can generate the same type of wave, which is an antenna [4]. This antenna functions as both a transmitter, emitting electromagnetic energy, and a receiver, collecting

OPEN ACCESS

backscattered signals that penetrate objects. The collected signals are then processed and analyzed to create imaging images [5]. The Council of the European Union [6] has regulated radiation exposure to allow for operation within the frequency range of 3.1–10.6 GHz, with a Specific Absorption Rate (SAR) of 1.6 W/kg [7]. Abnormal tissue absorbs more electromagnetic energy than normal tissue, resulting in a noticeable difference in the imaging image. Ideally, a good antenna should possess high gain to detect tissue abnormalities and have high bandwidth, making it suitable for MWI systems [8,9].

The AVA is a potential candidate for use in MWI due to several advantages [10]. Firstly, AVA boasts a broad and even radiation pattern, facilitating improved detection of areas within the human body, supported by its twin-patch curve structure, which influences bandwidth, gain, and signal operation [11]. Secondly, AVA can operate over a wide frequency range, resulting in higher-resolution images. Thirdly, AVA is relatively easy to manufacture and can be used at an affordable cost. These advantages position AVA as a promising option for MWI systems [12].

Research and testing regarding the use of AVA in MWI have been conducted by Salleh et al. [4]. They provided a configuration of the AVA design for anomaly detection (based on 8 antennas) within the frequency range of 2.06–2.61 GHz, resulting in a gain of 2.48 dBi, a bandwidth of 23.5%, and imaging images. A similar study was also carried out by Özmen and Kurt [13], who provided a configuration for the AVA design (based on one antenna). They incorporated a Koch fractal to detect anomalies (2 mm in size) in the form of 3D breast cancer at a distance of 50 mm, within a frequency range of 3.05–12.2 GHz. Detection was performed at a target frequency of 9 GHz, yielding a gain of 8.2 dBi, a 60.5% bandwidth, RL (Return Loss) of -18 dB, and imaging images. Another study, conducted by Wang et al. [14], employed an AVA design configuration to detect the presence of objects or human positions at a frequency range of 3-10 GHz, with object positions at distances ranging from 0.84 to 1 m. The target frequency for detection was > 6 GHz, resulting in a gain of 11.8 dBi, a 130% bandwidth, RL of -12 dB, and S21 analysis.

However, previous research does not clearly address the SAR value as a limitation in the absorption of electromagnetic energy from the body to the artificial body (Phantom). Additionally, Wang et al. [14] explained S21 at long distances but did not provide an explanation for objects at close range. This article will focus on the configuration and structural design analysis of AVA as a device supporting the MWI method for medical imaging. This analysis will include the S11 test (antenna characterization) and the S21 test (antenna penetration) for three types of processing: without a phantom (antenna only), with a water phantom, and with a water phantom containing an anomaly (abnormal network). Furthermore, the article will analyze the SAR results from the Phantom in the near detection area obtained after the S21 test.

METHOD
Object

The study will utilize two AVAs, an FR-4 substrate (for the AVA patch), a phantom (water), anomalies (balls), and an area for simulation as objects. The types and object permittivity values are shown in Table 1.

Table 1. The Relative Permittivity Value of the Object

Object	Relative Permittivity (ε_o)	Description

Susbtrate	4.3	FR-4
Phantom	78.0	Water
Anomalies	4.3	FR-4
Area	1.0	Air

Design

The AVA configuration used Flame Retardant-4 (FR-4) as a substrate with a thickness of 1.6 mm (ε_r = 4.3, tan δ = 0.025). The dimensions of the antenna rectangle are 60×40 mm^2. The patch antenna uses copper material. The feedline dimensions 38.16×1 mm^2, and the impedance value is 50 Ω. Curve A (the exponential part with long curvature) on the patch antenna is created using the Equation 1 [2].

$$x(t) = t + A1 , \ y(t) = A + e^{(m.t)} \tag{1}$$

Meanwhile, curve B (the exponential part with a short curve) is created using the Equation 2 [2]:

$$x(t) = t + B1 , \ y(t) = B + e^{(n.t)} \tag{2}$$

Where $x(t)$ is a function used to horizontally position the line adjusted to equations (1 & 2), and $y(t)$ is used for vertical positioning in Equations (1 & 2). Additionally, t itself is a function that adds or subtracts lines in accordance with the equations provided [15].
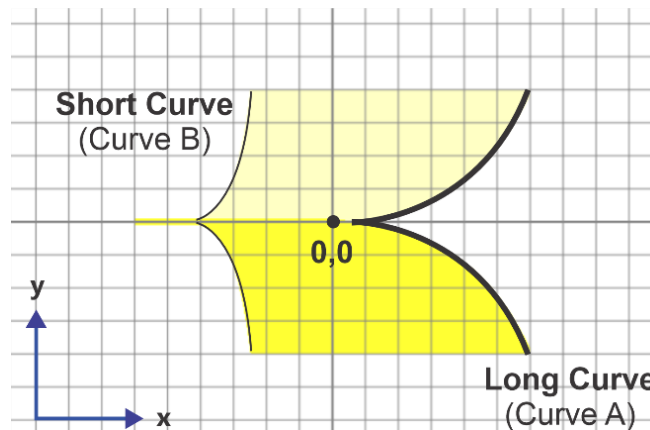
Figure 1. Coordinates on the AVA Design for Short Curve (Curve B) and Long Curve (Curve A)

The optimization of the AVA design involves specific parameters aimed at achieving a wide output bandwidth, high gain, and effective radiation direction during characterization tests and tests using phantom objects [16,17]. The curvature of the patch is designed to maintain a constant beamwidth within the signal's operating range in the required frequency spectrum. The parallel feedline configuration on the twin patch plays a significant role when AVA operates at high frequencies, functioning as a traveling wave radiator—a waveguide during the main transmission, characteristic of a non-resonant antenna with an ultra-wide bandwidth (UWB) range in a single direction. This configuration effort also enhances the cutoff for high frequencies. In contrast, when the AVA operates at low frequencies, it functions as a resonating antenna. The effectiveness of the radiation pattern of the antenna depends on resonance, where the width of the taper's mouth equals half of the effective wavelength (λ_{maks})[12,18,19]. The objectives of this

study include achieving bandwidth values exceeding 20%, gain greater than 5 dB, and a Return Loss (RL) below -10 dB.

In order to achieve the desired target, the dimensions of the AVA in this study underwent a modification in the configuration of the exponential section. This alteration aimed to widen the sharp mouth of the AVA, differing from the previous work by Lu et al. [2]. Lu et al.'s [2] design parameters were derived through an optimization procedure using full-wave electromagnetic simulations, whereas our research employed the time and frequency domain method. The radiation flares were constructed utilizing the exponential equation [2]:

$$Z = \pm A \times e^{p*(x-B)} + C \tag{3}$$

Where Z is a function employed to concurrently integrate the positions of the x and y axes during curve optimization. A and p serve as magnification factors for the curve, while B is used for horizontal line adjustment, and C is applied for vertical line adjustment. A comparison between our AVA (antenna in this study) and the antenna by Lu et al. [2] will be presented in Table 2 and Figure 2.

(a)   **(b)**
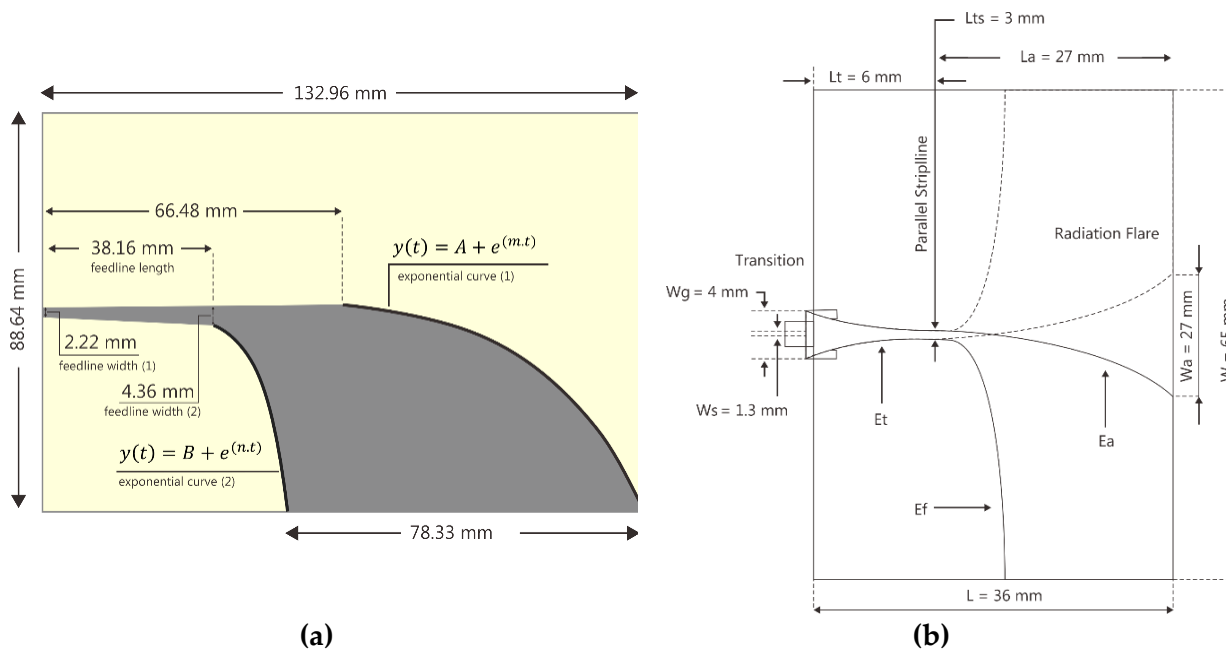
Figure 2. (a) AVA Design in This Study and (b) Lu et al.'s Antenna Design [2] for Optimization Parameters

Table 2. Comparision of Optimization Parameters Antenna

AVA			Lu et al antenna's		
Parameter	Value (mm)	Description	Parameter	Value (mm)/ Equation	Description
A	-1.5	The position of curve A on the Y-axis	p	$p_t = -1.82;$ $p_a = 0.094;$ $p_f = 0.487;$	-
B	-0.5	The position of curve B on the Y-axis	B	$0;$ $l_t + l_{ts};$ $l_t + l_{ts};$	l_t: feedline length; l_{ts}: width of the feedline;
$A1$	0	The position of curve A on the X-axis	C	$\frac{w_g}{2} - A_t;$ $-\frac{w_{ts}}{2} - A_a;$ $\frac{w_{ts}}{2} - A_f;$	w_g: width of the bottom patch of the feedline;
$B1$	-20	The position of curve B on the X-axis	Curve	$E_t;$ $E_a;$ $E_f;$	--
h	1.6	Substrate Height	A	$\frac{w_{ts} - w_g}{2 \times (e^{p_t \times l_t} - 1)};$ $\frac{w_{ts} + w_a}{2 \times (e^{p_a \times l_a} - 1)};$ A_f	w_a: wide mouth curve; l_a: length of feedline to curve;
k	8.01	Feedline Constant			
m	0.101	The Value of Curve Exponential (1)			
n	0.4	The Value of Curve Exponential (2)			

Measurement of Scattering Parameter (S11 & S21)

The simulation of the AVA design (as depicted in Figure 2a) was conducted using the CST Studio Suite 2019 application. The simulation commenced with measurements of S11 and S21, employing several initial settings, which included a simulation frequency range of 6-10 GHz, a time domain solver accuracy of -20 dB, and an impedance value of 50 ohms. In the first measurement (see Figure 3), the primary focus was on S11, which pertains to characterizing one antenna as the subject of the simulation test. The objective was to assess the antenna's performance values [20,21].
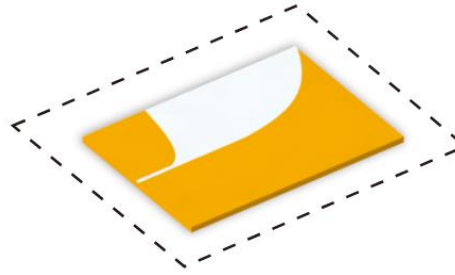
Figure 3. AVA Characterization Simulation (S11)

In the second measurement (see Figure 4), the emphasis shifted to the S21 parameter, representing the power transfer between two antennas. This experiment involved the use of two antennas as test subjects. The primary objective of this test was to observe signal propagation and attenuation when there were no physical obstructions between the antennas. The experiment was conducted with the two antennas positioned approximately 50 mm apart. This specific distance was selected to analyze the behavior of electromagnetic signals over short distances. By maintaining the antennas nearby, the measurement aimed to assess how effectively the signal could penetrate the free space between them [22].
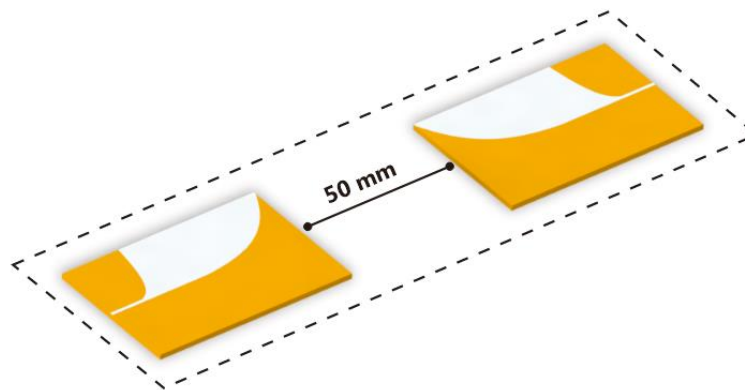
Figure 4. Simulation S21 without Phantom

In the third measurement (see Figure 5), the focus continued to be on the S21 parameter, representing the power transfer between the two antennas. However, this time, a different scenario was introduced to simulate the presence of an object between the antennas. A water phantom with dimensions of 20 mm³ was positioned between the two antennas. The water phantom served as a biological medium to investigate how the signal would behave when propagating through a material with dielectric properties similar to biological tissues. Such experiments are crucial in evaluating the performance of antenna systems in medical applications, where devices may need to pass through body tissues non-invasively. The water phantom was placed at a distance of 5 mm from the antennas [23,24].
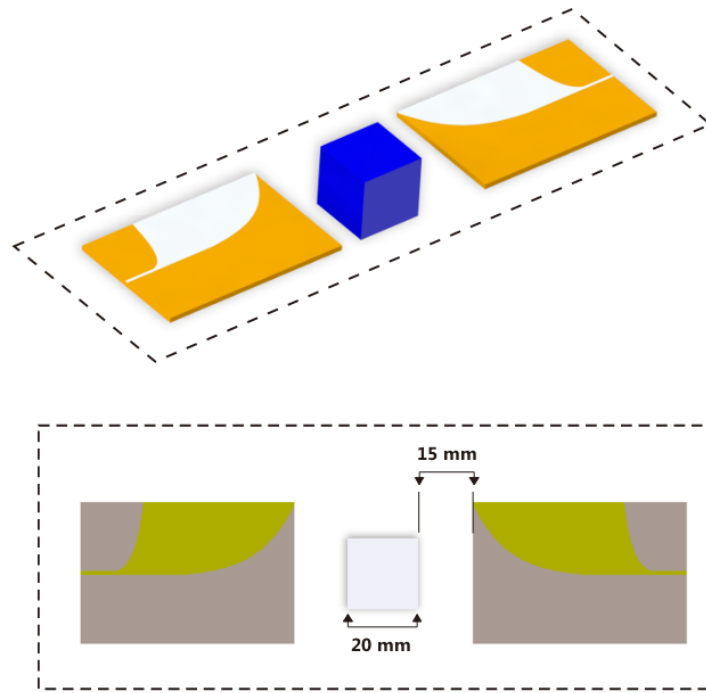
Figure 5. Simulation S21 with The Water Phantom

In the fourth measurement (see Figure 6), S21 was measured by introducing an anomaly into the water phantom. The anomaly had a diameter of 10 mm [25].
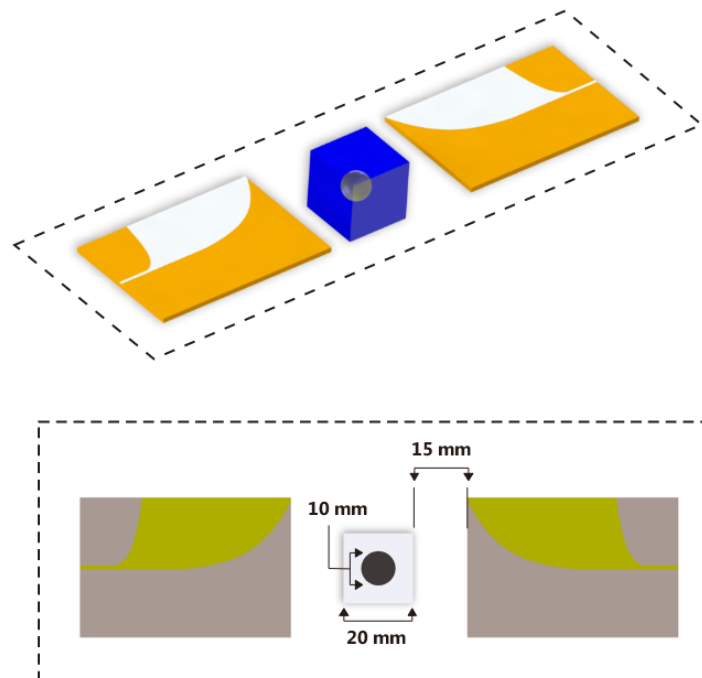
Figure 6. Simulation S21 with The Water Phantom

Measurement of Specific Absorption Rate (SAR)

According to Ahmed, SAR is defined as a derived form of the energy level that can be absorbed by the body (Phantom) against the time interval from the absorption period where

there is an increase in body mass volume due to exposure to a specific density value. The equation is shown by Equation 3 [8]:

$$SAR = \frac{d}{dt}\left(\frac{dw}{dm}\right) \tag{3}$$

So, based on the derivative of equation 3, dW/dm is the derivative of power per mass, and the SAR unit is watts per kilogram (W/kg) or milliwatts per gram (mW/g). Meanwhile, the definition of SAR based on the induction of the electromagnetic field is shown in Equation 4 [26]:

$$SAR = \frac{\sigma.E^2}{\rho} \tag{4}$$

Where σ indicates the value of the conductivity of the tissue (S/m), E represents the value of the internal electromagnetic energy (V/m), and is the density of the tissue mass (kg/m³). The SAR value in equation 4 calculates exposure to tissue mass on a scale per unit of 1 g or 10 g [8,9,26,27].

RESULTS AND DISCUSSION

Analysis of S11

The graphical results of the characterization simulation (S11) on a single antenna are shown in Figure 7, where the usable frequency area is under -10 dB. Generally, a good or efficient S11 value for an antenna should be under -10 dB, where at an S11 value of -10 dB, about 10% of the power delivered to the antenna will be reflected. The antenna will absorb or emit about 90% of the power. If the value of S11 is worse than -10 dB, then more power is reflected in the source, and the antenna is less efficient. Therefore, S11 -10 dB is a standard or benchmark commonly used to indicate an antenna's quality or efficiency [28,29].
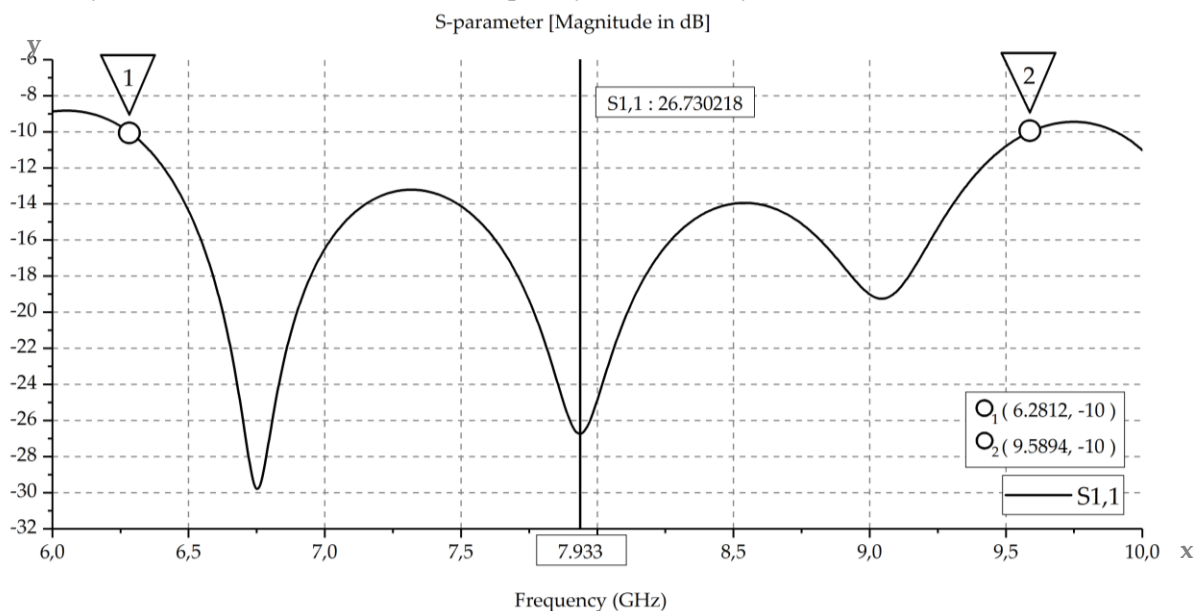
Figure 7. Simulation S11 with The Water Phantom

The simulation test results for one antenna in Figure 2 are characterized by an S11 graph in a return loss scale of -10 dB, as shown in Figure 7. The graph displays points 1 (6.2812 GHz, -10 dB) and 2 (9.8894 GHz, -10 dB). These points serve as reference measurements for several parameters listed in Table 3.

Table 3. Characterization Parameters for AVA

Parameter	Value
VSWR	1.096 ~ 1,1
Gain	5.16 dB
Bandwidth	41.61%
Directivity	6.484 dBi
Frequency Target	7.933 GHz
Return Loss	-26.73 dB

This antenna demonstrates excellent performance compared to similar experiments conducted by Salleh et al. [4]. Their experiment reported a directivity of only 2.48 dBi, indicating that this antenna exhibits superior energy concentration towards the front direction. Furthermore, their experiment reported a narrower bandwidth range of only 23.5%, whereas this antenna operates efficiently within a broader frequency range.

Additionally, this antenna's negative return loss value of -26.73 dB is considerably lower than the -18 dB value reported in the Özmen & Kurt experiment [13]. This result indicates a better impedance match for this antenna, resulting in less power being reflected to the source. These results underscore that this antenna is a more efficient and high-performing choice for its intended application [15,28,30].

Analysis of S21

The graph displaying the results from the S21 experiment is presented in Figure 8. This graph combines all the S21 simulations into one, facilitating easier comparisons of the penetration performance conducted in the tests depicted in Figures 4, 5, and 6.
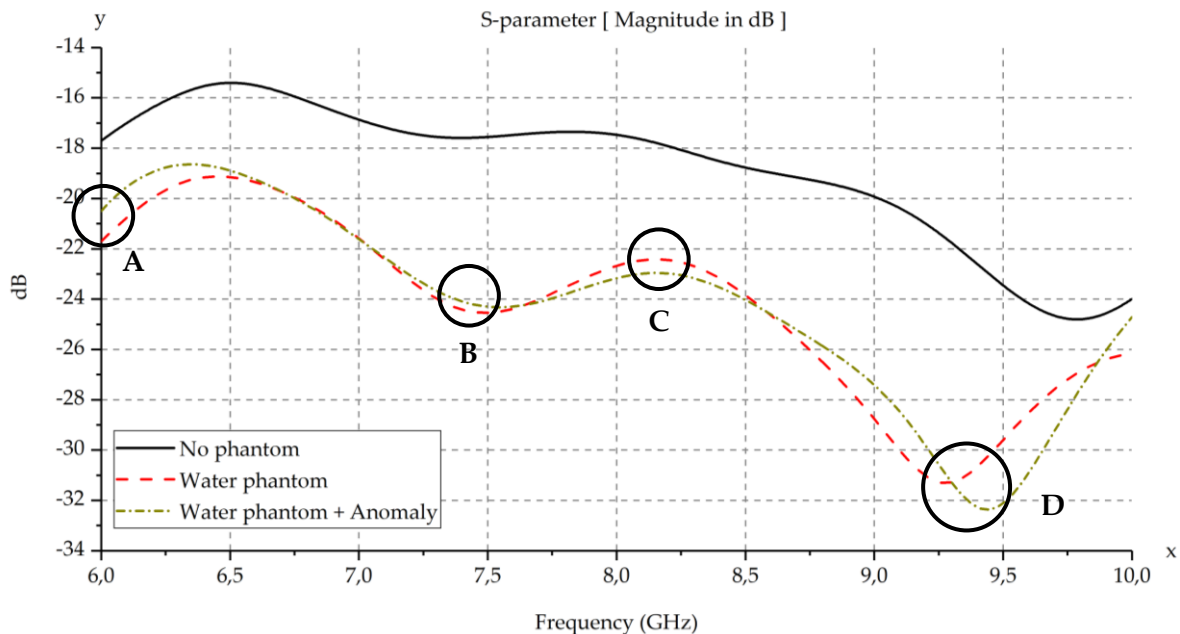
Figure 8. S-Parameter Graph (S21) AVA Simulation Test

The tests conducted on the water phantom section, both without the anomaly and with the addition of the anomaly, have revealed a noticeable shift in the graph. This shift is a result of the antenna's detection of abnormalities within the water phantom object [31]. To simulate these irregularities and facilitate detection testing, a method based on the difference in relative

permittivity values between water and air anomalies was employed. The relative permittivity value of the air anomaly is significantly lower than that of water, making it easier for the antenna to detect and causing a shift in the S-parameter values [32,33]. The coordinate points representing this shift are presented in Table 4.

Table 4. Coordinate Point Shift on Graph S21

Point	ΔX-axis (GHz)	ΔY-axis (dB)	Coordinate Shift (x,y)
A	(6.00) – (6.00) = 0.00	(-21.47) - (-20.28) = -1.19	(0.00, -1.19)
B	(7.37) – (7.37) = 0.00	(-24.31) - (-23.97) = -0.34	(0.00, -0.34)
C	(8.16) – (8.16) = 0.00	(-22.89) - (-22.38) = -0.51	(0.00, -0.51)
D	(9.43) – (9.26) = 0.17	(-32.46) - (-31.56) = -0.85	(0.17, -0.85)

Previous research conducted by Wang et al. [34] discovered that anomalous antenna penetration in the liver phantom resulted in differences in the S-parameter graph. These differences overlapped each other in various manipulations (presence or absence of the phantom), where the object absorbed the electromagnetic signal. Artificial intelligence, such as the phantom, can be influenced by anomalous permittivity. The variation in permittivity between the anomaly and the surrounding tissue can lead to differences in the intensity of the reflected and transmitted fields at the boundary surface [3–5,20]. Consequently, it is essential to take into account the material parameters of anomalous objects in the design of medical imaging systems and the interpretation of data. Scattering plots can illustrate how electromagnetic waves propagate in a medium and identify anomalies in tissues, such as tumors or cysts, providing valuable information for disease detection and diagnosis [9,30].

Analysis of SAR (Specific Absorption Rate)

In a previous study, Jamlos et al. [26] employed a patch antenna operating within the frequency range of 1.6-10.8 GHz. The antenna demonstrated a gain ranging from 3.2 dB to 14.1 dB. The study involved SAR testing with a regulated antenna distance of 100 mm from the head tumor area. The object used in the experiment resembled a cube filled with liquid, featuring a relative permittivity value (ε_r) of 63.2, and it included an anomaly with a relative permittivity (ε_r) of 2.3. The results indicated that the resulting SAR level was 1.47 W/kg.

In this article, the AVA was tested within the frequency range of 6-10 GHz, demonstrating a gain of 5.16 dB. The antenna was positioned 15 mm from the phantom object being tested, which took the form of a cube filled with water, having a relative permittivity (ε_r) of 78. An anomaly in the shape of a ball was introduced into the phantom, composed of air with a relative permittivity (ε_r) is 1. The results, obtained through simulations using the CST Studio Suite 2019 application, indicated an absorption level of 0.26 W/kg.

Both studies employed distinct types of antennas and objects featuring different relative permittivity values. However, they demonstrate that manipulating relative permittivity values can facilitate detection testing. Additionally, the SAR absorption levels observed in both studies fall within the range regulated by the Council of the European Union [8,9,33].

This research is constrained to specific operating frequencies in accordance with the regulations of The Council of the European Union, within the range of 3.1 – 10.6 GHz [6]. The scope is currently limited to the territory of simulation. The target limits in the AVA simulation

that must be achieved in this study include bandwidth values exceeding 20%, gain greater than 5 dB, and a Return Loss (RL) below -10 dB.

The next development phase for this research involves enhancing simulation accuracy by incorporating more complex and realistic environmental factors, such as wave disturbance modeling, to align closer with actual conditions. Additionally, expanding the variety of phantom and anomalous materials used is crucial to deepen the understanding and applicability of AVA designs for medical scanning applications. Further research focus could be directed toward optimizing the Vivaldi antenna geometry. Exploring ways to increase the radiation efficiency and gain of the antenna at a given operating frequency can lead to improved antenna performance. Moreover, considering polarization adjustments is essential to cater to the specific needs of medical scanning applications.

Advancements in antenna technology promise improvements in various areas, such as electromagnetic wave propagation and signal processing. This research has the potential to contribute significantly to the understanding of wave behavior and antenna characteristics, fostering new insights and knowledge in the domain of electromagnetic theory and antenna engineering. Particularly within medical physics, these advancements may drive innovation in medical imaging by introducing a new and optimized AVA design. The primary objective is to enhance antenna sensitivity, ultimately contributing to early diagnosis and treatment of internal diseases.

CONCLUSION

In this study, the optimized AVA structure plays a crucial role in enhancing the S11 parameters, resulting in a significant increase in bandwidth (41.61%), gain (5.16 dB), and a reduction in return loss (-26.73 dB), all of which are targeted performance characterization parameters. The S21 graph illustrates subtle yet discernible differences between overlapping simulated graphs using microwaves, providing evidence of the anomaly. Additionally, the SAR value of 0.26 W/kg remains within reasonable limits for MWI penetration. In conclusion, the AVA design exhibits the potential to serve as an effective anomaly detection tool in microwave-based medical imaging applications.

ACKNOWLEDGMENT

AUTHOR CONTRIBUTIONS

Daffa Mahendra and Endarko: Conceptualization, Methodology, Validation, and prepared and wrote the original draft; Daffa Mahendra, Randy Ivanal Hakim, and Endarko: Methodology, Formal Analysis, data collection, and Visualization.

DECLARATION OF COMPETING INTEREST

The authors declare that they have no known competing financial interests or personal relationships that could have appeared to influence the work reported in this paper.

REFERENCES

[1] Ameer W, Awan D, Bashir S, and Waheed A. Use of Directional UWB Antenna for Lung Tumour Detection. *Proceeding of International Conference on Advancements in Computational Sciences (ICACS)*. Lahore: IEEE. 2019; 1–5. DOI: https://doi.org/10.23919/ICACS.2019.8689137.

[2] Lu Y, Fang C and Ye X. Antipodal Vivaldi Antenna Designed for Microwave Imaging System. *2019 International Applied Computational Electromagnetics Society Symposium - China (ACES)*. Nanjing, China: IEEE. 2019; 1–2. DOI: https://doi.org/10.23919/ACES48530.2019.9060467.

[3] Islam MT, Mahmud MZ, Islam MT, Kibria S, and Samsuzzaman M. A Low Cost and Portable Microwave Imaging System for Breast Tumor Detection Using UWB Directional Antenna Array. *Scientific Reports*. 2019; **9**(1): 15491. DOI: https://doi.org/10.1038/s41598-019-51620-z.

[4] Salleh A, Yang CC, Singh M, Singh J, and Islam MT. Development of Antipodal Vivaldi Antenna for Microwave Brain Stroke Imaging System. *International Journal of Engineering & Technology*. 2019; **8**(3): 162–168. DOI: http://dx.doi.org/10.14419/ijet.v8i3.19933.

[5] Samsuzzaman Md, et al. A 16-modified Antipodal Vivaldi Antenna Array for Microwave-based Breast Tumor Imaging Applications. *Microwave and Optical Technology Letters*. 2019; **61**(9): 2110–2118. DOI: https://doi.org/10.1002/mop.31873.

[6] Council of the European Union. *1999/519/EC: Council Recommendation of 12 July 1999 on the Limitation of Exposure of the General Public to Electromagnetic Fields (0 Hz to 300 GHz*. Luxemburg: EUR-Lex. 1999; 59–70. Available from: http://data.europa.eu/eli/reco/1999/519/oj.

[7] Federal Communications Commission (FCC). *Revision of Part 15 of the Commission's Rules Regarding Ultra-Wideband Transmission System*. Washigton DC: FCC; 2002. Available from: https://www.fcc.gov/document/revision-part-15-commissions-rules-regarding-ultra-wideband-7.

[8] Ahmed A. Specific Absorption Rate (SAR) Simulated for Square Patch Antenna of Head Tissues. *Engineering and Technology Journal*. 2018; **36**(5A): 209–513. DOI: https://doi.org/10.30684/etj.36.5A.5.

[9] Prakash P and Srimathveeravalli G. *Principles and Technologies for Electromagnetic Energy Based Therapies*. Cambridge: Academic Press; 2021.

[10] McMillan RW and Bohlander RA. *An Investigation of Millimeter Wave Propagation in the Atmosphere: Measurement Program*. Research Report. Atlanta: Georgia Tech Research Institute; 1987. Available from: https://apps.dtic.mil/sti/citations/ADA184837.

[11] Gazit E. Improved Design of the Vivaldi Antenna. *IEE Proceedings H (Microwaves, Antennas and Propagation)*. 1988; **135**(2): 89-92. DOI: https://doi.org/10.1049/ip-h-2.1988.0020.

[12] Parveen F and Wahid P. Design of Miniaturized Antipodal Vivaldi Antennas for Wideband Microwave Imaging of the Head. *Electronics*. 2022; **11**(14): 2258. DOI: https://doi.org/10.3390/electronics11142258.

[13] Özmen H and Kurt MB. Radar-Based Microwave Breast Cancer Detection System with a High-Performance Ultrawide Band Antipodal Vivaldi Antenna. *Turkish Journal of Electrical Engineering and Computer Science*. 2021; **29**(5): 2326–2345. DOI: https://doi.org/10.3906/elk-2010-49.

[14] Wang J, Liu J, Hou K and Li Y. A Novel Antipodal Vivaldi Antenna for Ultra-Wideband Far-Field Detection. *AEU - International Journal of Electronics and Communications*. 2023; **164**: 154626. DOI: https://doi.org/10.1016/j.aeue.2023.154626.

[15] Balaji A, Karthi J, Chinnamal V, Malarvizhi C, and Vanaja S. A Unique Technique to Improve the Performance of Antipodal Vivaldi Antenna for Microwave Imaging Application. *IOP Conference Series: Materials Science and Engineering*. 2021; **1055**(1): 012100. DOI: https://doi.org/10.1088/1757-899X/1055/1/012100.

[16] Rafique U, Pisa S, Cicchetti R, Testa O, and Cavagnaro M. Ultra-Wideband Antennas for Biomedical Imaging Applications: A Survey. *Sensors*. 2022; **22**(9): 3230. DOI: https://doi.org/10.3390/s22093230.

[17] Wang M, et al. A Compact Slot-Loaded Antipodal Vivaldi Antenna for a Microwave Imaging System to Monitor Liver Microwave Thermal Ablation. *IEEE Open Journal of Antennas and Propagation*. 2022; **3**: 700–708. DOI: https://doi.org/10.1109/OJAP.2022.3183750.

[18] Dixit AS and Kumar S. A Survey of Performance Enhancement Techniques of Antipodal Vivaldi Antenna. *IEEE Access*. 2020; **8**: 45774–45796. DOI: http://dx.doi.org/10.1109/ACCESS.2020.2977167.

[19] Hasim NS, et al. A Slotted UWB Antipodal Vivaldi Antenna for Microwave Imaging Application. *Progress In Electromagnetics Research M*. 2019; **80**: 35–43. DOI: http://dx.doi.org/10.2528/PIERM18121201.

[20] Lalitha K and Manjula J. Non-Invasive Microwave Head Imaging to Detect Tumors and to Estimate Their Size and Location. *Physics in Medicine*. 2022; **13**: 100047. DOI: https://doi.org/10.1016/j.phmed.2022.100047.

[21] Tangwachirapan S, Sawangsri P, Pinitkiatisakul P, Thongdit P, and Thaiwirot W. Breast Cancer Detection Based Microwave Imaging Using Single Antipodal Vivaldi Antenna. *Research, Invention, and Innovation Congress: Innovative Electricals and Electronics (RI2C)*. Bangkok: IEEE. 2022; 97–100. DOI: https://doi.org/10.1109/RI2C56397.2022.9910316.

[22] Guruswamy S, Chinniah R and Thangavelu K. A Printed Compact UWB Vivaldi Antenna with Hemi Cylindrical Slots and Directors for Microwave Imaging Applications. *AEU - International Journal of Electronics and Communications*. 2019; **110**: 152870. DOI: https://doi.org/10.1016/j.aeue.2019.152870.

[23] Alageea R and Assalemb A. Brain Cancer Detection Using U-Shaped Slot VIVALDI Antenna and Confocal Radar Based Microwave Imaging Algorithm. *American Scientific Research Journal for Engineering, Technology, and Sciences (ASRJETS)*. 2020; **66**(1): 1–13. Available from:
https://asrjetsjournal.org/index.php/American_Scientific_Journal/article/view/5651.

[24] Birwal A, Patel K and Singh S. A Directional Wide-Band Antipodal Vivaldi Antenna for Imaging Applications. *Progress In Electromagnetics Research C*. 2022; **127**: 227–237. DOI: http://dx.doi.org/10.2528/PIERC22102201.

[25] Asok AO, J. GNS and Dey S. Non-invasive Breast Tumor Detection with Antipodal Vivaldi Antenna Using Monostatic Approach. *International Journal of RF and Microwave Computer-Aided Engineering*. 2022; **32**(12): e23539. DOI: http://dx.doi.org/10.1002/mmce.23539.

[26] Jamlos MA, Mustafa WA, Khairunizam W, Zunaidi, I, Razlan ZM, and Shahriman AB. Tumor Detection via Specific Absorption Rate Technique Using Ultra-Wideband Antenna. *IOP Conference Series: Materials Science and Engineering*. 2019; **557**(1): 012024. DOI: https://doi.org/10.1088/1757-899X/557/1/012024.

[27] Susila M, et al. Investigations of Specific Absorption Rate and Temperature Variations for an UWB Antenna for Wireless Applications. *Progress In Electromagnetics Research M*. 2019; **78**: 83–92. DOI: http://dx.doi.org/10.2528/PIERM18111603.

[28] Balanis CA. *Antenna Theory: Analysis and Design*. New York: John Wiley; 2016.

[29] Paul L and Islam MM. A Super Wideband Directional Compact Vivaldi Antenna for Lower 5G and Satellite Applications. *International Journal of Antennas and Propagation*. 2021; **2021**: 8933103. DOI: https://doi.org/10.1155/2021/8933103.

[30] Chiappe M and Gragnani GL. Vivaldi Antennas for Microwave Imaging: Theoretical Analysis and Design Considerations. *IEEE Transactions on Instrumentation and Measurement*. 2006; **55**(6): 1885–1891. DOI: http://dx.doi.org/10.1109/TIM.2006.884289.

[31] Sohani B, et al. Detection of Haemorrhagic Stroke in Simulation and Realistic 3-D Human Head Phantom Using Microwave Imaging. *Biomedical Signal Processing and Control*. 2020; **61**: 102001. DOI: https://doi.org/10.1016/j.bspc.2020.102001.

[32] Yazid MYI, et al. A Sierpinski Arrowhead Curve Slot Vivaldi Antenna for Microwave Head Imaging System. *IEEE Access*. 2023; **11**: 32335–32347. DOI: https://doi.org/10.1109/ACCESS.2023.3262607.

[33] Hekal S, Asaad FE, Mansour HM and Shehata GS. Microwave Imaging System for Breast Cancer Detection Using Merit Toolbox. *40th National Radio Science Conference (NRSC)*. Giza: IEEE. 2023; 327–336. DOI: https://doi.org/10.1109/NRSC58893.2023.10152940.

[34] Wang M, Crocco L and Cavagnaro M. Antipodal Vivaldi Antenna with Ceramic Cone Lens for Biomedical Microwave Imaging Systems. *15th European Conference on Antennas and Propagation (EuCAP)*. Dusselford, Germany: IEEE. 2021; 1–5. DOI: https://doi.org/10.23919/EuCAP51087.2021.9411294.